Data analysis of the Scattering Study for the PiENu Experiment

for Physics 449

by

Michael Jansz

A THESIS SUBMITTED IN PARTIAL FULFILMENT OF
THE REQUIREMENTS FOR THE DEGREE OF

Bachelor of Science (Hons)

in

Faculty of Science

(Physics & Astronomy)

The University Of British Columbia

(Vancouver, Canada)

April, 2008

Abstract

The PiENu (**pi**on $\rightarrow$ **e**lectron + **neu**trino) experiment is measuring the $\Gamma(\pi \rightarrow e\nu)/\Gamma(\pi \rightarrow \mu\nu)$ branching ratio. The goal is an increase in precision to the level of $< 0.1\%$, providing a strong test of lepton universality in the Standard Model. This improvement in precision on past measurements will be gained on many fronts. First, a revised setup will improve statistics, reducing statistical uncertainties. Second, improvements in particle identification will reduce systematic uncertainties. Finally, extensive Monte-Carlo (MC) simulation of the setup will reduce the uncertainty due to energy-dependent scattering effects. In order to reduce this uncertainty, a preliminary beamtest has been conducted, in which data was collected with several variations on the experimental setup. This data was analyzed to determine the effects of scattering on the passage of the positrons through the apparatus, allowing a verification of the simulations, thus reducing uncertainty. This report outlines the data analysis used in this scattering study.

Table of Contents

List of Tables

List of Figures

Acknowledgements

I would like to thank Aleksey Sher and Douglas Bryman for their help and guidance with this research project. Their patience and help was much appreciated during the analysis of the data as well as the writing of this report.

Statement of Co-Authorship

This project is only a small part of a larger experiment, and the data analysis relies heavily on the work of many people.

- Kaoru Yamada whose example in past analysis provided important guidance while undertaking this project.
- Fabrice Retiere who created the script that processed the raw data to produce a form suitable for this analysis.
- Aleksey Sher and Douglas Bryman for their guidance during this project and their contributions to the composition of this report.
- The entire PiENu team for their work with the acquisition of this data.

Chapter 1

Introduction

The PiENu experiment is a precise measurement of the $\Gamma(\pi \to e\nu)/\Gamma(\pi \to \mu\nu)$ branching ratio. The goal is an uncertainty of less than 0.1%, providing a strong test of lepton universality in the Standard Model. This precision is an improvement by at least a factor of four from previous experiments and will be achieved through several improvements–one of which is the completion of a "Scattering Study." This scattering study will provide a better understanding of the effects of positron scattering in the apparatus. This will provide confidence in the GEANT4 Monte Carlo simulation used to predict the acceptance of the apparatus, thus decreasing the uncertainty in the final measurement. This report is concerned with the analysis of the data from this Scattering Study. The purpose of the report is threefold. It will:

1. Document the analysis process for future reference and provide an outline for subsequent analysis.

2. Provide confidence in the results by explaining the rationale behind the analysis and providing necessary statistics.

3. Provide a summary of the final results of the analysis.

This report is intended to be "self contained"; however, some background would certainly be beneficial. In particular, familiarity with particle physics may be helpful for the Theory and Scientific Motivation sections, and an understanding of the PiENu experiment would make the Analysis section more meaningful.

Chapter 2

Scientific Motivation

In the Standard Model (SM) of the fundamental particles and their interactions there are three generations of leptons, shown in blue in figure 2.1. The three charged particles are the electron (e), the muon (μ), and the tau (τ). In the SM, these three particles are assumed to be identical in every respect, except that their masses differ. This gauge invariance among the different generations is referred to as lepton universality.

Lepton universality is embedded in the SM; however, it fails to explain why three generations exist or why they must interact identically. The PiENu experiment intends to challenge this aspect of the SM by measuring the relative electroweak gauge interactions of the electron and the muon for comparison with SM prediction.

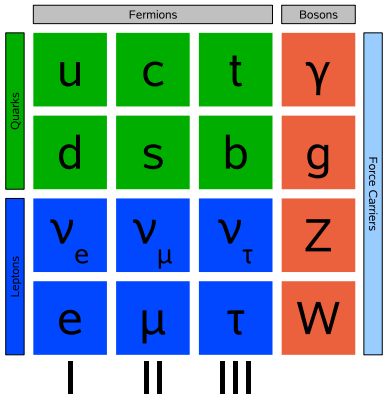

Figure 2.1: Diagram showing the three lepton generations.

Pion decay provides a unique opportunity to test the SM, as the branching ratio $R_{\mu/e} = \frac{\Gamma(\pi \to e\nu)}{\Gamma(\pi \to \mu\nu)}$ is both precisely measurable and calculable. The most recent calculation, including all known effects and conservative bounds for all unknown effects, places this branching ratio at

$$R^{th}_{\mu/e} = (1.2352 \pm 0.0005) \times 10^{-4}$$

as calculated by Marciano and Sirlin. [5]

In the past, three experiments have been done to measure this branching ratio. Their results are summarized in table 2.1 below.

The two most recent measurements provide an uncertainty of roughly 0.4%. Although this uncertainty is quite small, it is still too large to truly challenge the SM. This experiment intends to measure the $R_{\mu/e}$ branching ratio to within $< 0.1\%$–an improvement of at least a factor of four. At this level, the experimental uncertainty will approach the level of theoretical uncertainty allowing a statistically significant comparison. Agreement at this level would provide strong

Location	Year	$R^{exp}_{\mu/e} \pm (stat) \pm (syst)$	Ref.
TRIUMF	1986	1.218 ± 0.014	[6]
TRIUMF	1992	$1.2265 \pm 0.0034 \pm 0.0044$	[7]
PSI	1993	$1.2346 \pm 0.0035 \pm 0.0036$	[8]

Table 2.1: Past measurements of $R^{exp}_{\mu/e}$.

support for the SM and tight restraints on possible extension, whereas disagreement would be indicative of new physics. [9]

A discrepancy between theory and experiment would be indicative of physics beyond the standard model. The new physics could take many forms as the existence of separate gauge bosons for the different generations, charged lepton mixing, new charged Higgs scalars, or any new particle allowing scalar or pseudo-scalar interactions could affect the branching ratio. This experiment would not identify this new physics; however, it could help direct future searches. [9]

On the other hand, close agreement between $R^{th}_{\mu/e}$ and $R^{exp}_{\mu/e}$ would place tight constraints on extensions to the SM. In particular, the $R_{\mu/e}$ branching ratio is extremely sensitive to helicity-unsuppressed scalar and pseudo-scalar couplings due to the helicity suppression of the $\pi \to e\nu$ decay. Since the effect of such a particle would vary as $\frac{1}{m^2}$, where m is the mass of the particle, close agreement between theory and experiment would place a high lower bound on the mass of any new particle participating in these interactions. This provides an elegant means of probing mass scales as high as 1000TeV, while not requiring high energy beams. [10]

A precise measurement of $R_{\mu/e}$ to within 0.1% provides a direct test of the SM, and would have important implications regarding its extension, regardless of the outcome of the measurement.

Chapter 3

PiENu Procedure

The procedure of the PiENu experiment is very similar to that of the past experiments measuring the $\Gamma(\pi \rightarrow e\nu)/\Gamma(\pi \rightarrow \mu\nu)$ branching ratio. At the most basic level, the experiment involves stopping a sample of pions, allowing sufficient time for them to decay, and observing the decay products. The branching ratio is then computed by taking the ratio of the numbers of the two types of decays that were observed.

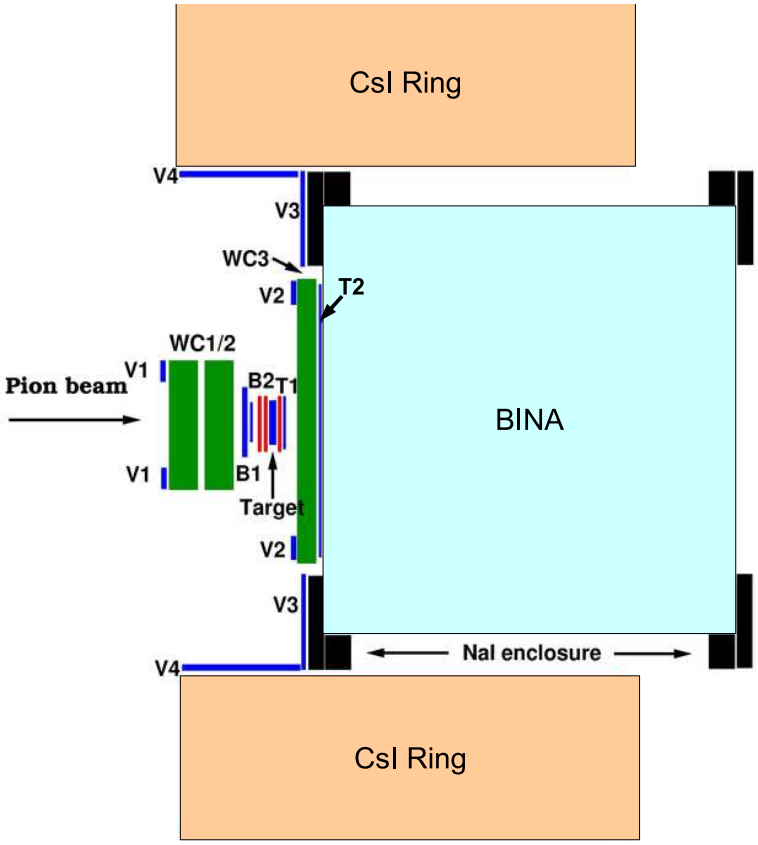

Figure 3.1: An aerial view of the PiENu apparatus. [4]

In reality, the experiment is much more complicated. The process begins with a beam of pions produced by the impact of a proton beam from the TRIUMF cyclotron on a graphite target. The beam intensity should be between $5 - 10 \times 10^4 \pi^+/s$ in order to maximize the event rate while minimizing pileup. Beam momentum must have a maximum variation of 1% to ensure that the pions stop in the center of the target. [10] The beam of pions enters the PiENu apparatus,

shown in figure 3.1. The pions then pass through a series of detectors and come to rest in a thin scintillating target. The pre-target detectors include scintillating beam (B) counters and wire chambers that measure the energy and position of the particles, respectively. After stopping in the target, the pions then decay via one of the $\pi \to \mu \to e$ or $\pi \to e$ decay chains. In either case, the final product is a positron, which exits in a random direction. Supposing the positron exits toward the BINA crystal, it then passes through a series of scintillating telescope (T) counters and one more wire chamber before it enters the crystal where its energy is precisely measured. The positron from the $\pi \to \mu \to e$ and $\pi \to e$ decays have characteristic energy distributions, so the number of each type of decay can be inferred from the positron energy distribution in the crystal.

The final complication in this process arises from the acceptance of the apparatus–the ratio of observed positron to produced positron. Due to small scattering effects in the telescope scintillators, the acceptances for the positrons from the different decay chains differ slightly and a small correction is needed. This correction involves a very elaborate computation with no analytical solution, requiring the use of Monte Carlo simulations to provide an estimate.

Chapter 4

Motivation for Scattering Study

Given that the uncertainty in past measurements was 0.4%, significant improvement must be made in the experimental procedure in order to achieve the desired 0.1% level. Table 4.1 shows the sources of uncertainty in the most recent TRIUMF measurement of $R^{exp}_{\mu/e}$. The PiENu experiment makes improvements in all of these areas to increase precision.

The largest contribution comes from statistical fluctuations in the raw branching ratio, which will be improved through a longer run time and a setup that increases the acceptance of the crystal. The second largest contribution comes from the tail correction, which refers to the fit to the energy in the crystal to determine the numbers of $\pi \to \mu \to e$ and $\pi \to e$ events. This will be reduced through innovative fitting methods and better statistics to achieve more reliable fits. This leaves the acceptance predictions of the MC simulation as the last major source of uncertainty. In order to achieve the anticipated improvement in the precision of the final branching ratio, a significant improvement must also be made here. For this reason, a preliminary study of the accuracy of the simulation is required to increase confidence in the simulation's predictions and reduce the associated uncertainty. It may also suggest improvements to the model, further decreasing the uncertainly due to the simulation.

To eliminate uncertainty in the simulated acceptances, the predictions of the model must be verified separately to ensure that it properly accounts for all scattering effects. For this reason, a "Scattering Study" was undertaken to verify the model's predictions. In particular, the dependence of scattering on the quantity of material, and the angle and energy of the incident positron were tested. Data was taken over a range of these conditions and the predicted acceptances must be compared to the experimentally determined values.

Verifying that the simulations correctly predict all three effects will allow for the reliable prediction of the acceptances for the $\pi \to \mu \to e$ and $\pi \to e$ positrons. The objective is to confirm the simulation predictions to within 10%. The typical correction accounting for the acceptances

Raw branching ratio	$1.1994 \pm 0.0034 \pm 0.0023$
Multiplicative corrections:	
Tail correction	1.0193 ± 0.0025
Pion stop time	0.9998 ± 0.0008
Time calibration	1.0000 ± 0.0003
Monte Carlo	1.0027 ± 0.0011
V1 veto	1.0009 ± 0.0005
WC inefficiency	0.9998 ± 0.0004
π lifetime	1.0000 ± 0.0009

Table 4.1: The sources of uncertainty in the 1992 TRIUMF measurement. [1]

is on the order of 1%, requiring an accuracy in the experimentally determined acceptances of at least 0.1%. [11] Only with analysis at this precision can a meaningful improvement to the simulation be made and the overall 0.1% precision be reached.

Chapter 5

Theory

5.1 Calculating $R^{th}_{\mu/e}$

To lowest order, the $R^{th}_{\mu/e}$ can be calculated as:

$$R^{th}_{\mu/e} = \frac{m_e(m_\pi - m_e)}{m_\mu(m_\pi - m_\mu)} = 1.28 \times 10^{-4}$$

where all incalculable and unknown factors cancel in the ratio due to the assumed gauge invariance of the electron and the muon. [12]

The addition of higher order terms allows for the inclusion of radiative and pion-structure dependent effects, resulting in a slight adjustment to the branching ratio. The radiative corrections were first calculated by Berman and Kinoshita, who showed that this correction is -3.7%. [13, 14] This result has since been confirmed by Goldman and Wilson, and Marciano and Sirlin through different approaches. [15, 16] More recent calculations, which include structure-dependent and inner-bremsstrahlung effects, have also been carried out by Marciano and Sirlin, giving the current theoretical value mentioned in the previous section. [5]

In order to measure any deviation from lepton universality, one must be able to extract the electroweak couplings of the electron and muon from the branching ratio $R_{\mu/e}$. To do so, we note that this branching ratio depends on the squares of these couplings, so we can write

$$R^{exp}_{\mu/e} = \left(\frac{g_e}{g_\mu}\right)^2 R^{th}_{\mu/e}$$

and compute the ratio $\frac{g_e}{g_\mu}$. [7] This allows one to extract a direct measure of any violation of universality from a measurement of $R^{exp}_{\mu/e}$.

5.2 Positron Scattering

If the relative acceptances of the $\pi \to e$ and $\pi \to \mu \to e$ positrons are not known exactly, the true branching ratio cannot be extracted from the raw numbers of each type of event. Although the two acceptances are the same to first order there are several higher order effects that cause the two to differ, making MC simulation to determine acceptances a necessity. These effects include multiple-coulomb- and Bhabha- scattering, bremsstrahlung, positron annihilation in flight, and the absorption of low energy positrons in scintillators. Although these effects are quite small, they are energy dependent and thus act differently on the $\pi \to e\nu$ and $\pi \to \mu \to e$ positrons. For this reason, their effects on the acceptances must be properly considered in order to minimize uncertainty due to the MC simulation.

5.2.1 Multiple-coulomb-scattering

Multiple-coulomb-scattering refers to the positron being redirected several times as it passes through a material (one of the T counters), due to interactions with the positive nuclei. This scattering has the potential to direct a positron into the crystal that would otherwise have missed ("in" scattering), or deflect a particle that would otherwise have entered the crystal ("out" scattering). In general, these effects tend to cancel, making the contribution from multiple-coulomb-scattering very small.

5.2.2 Bhabha-scattering

Bhabha-scattering refers to the process by which positron scatters off of an electron. The two particles collide and interchange roles kinematically. This has similar effects to coulomb-scattering.

5.2.3 Positron Annihilation

Positron annihilation refers to the collision of an electron and a positron resulting in the production two gamma rays. In this case the positron is 'lost' and will not be seen in the crystal. Low energy positron absorption refers to positrons that slow to a stop in a scintillator where they annihilate. This effect contributes only to "out" scattering.

5.2.4 Bremsstrahlung

Bremsstrahlung refers to the emission of a photon as a charged particle (i.e. a positron) undergoes acceleration. This acceleration could be caused by either of the scattering effects mentioned above. The emitted photon carries energy away from the charged particle, producing a decreased speed and potentially a change in direction. The decrease in speed is particularly important as it leads to an increased probability of annihilation and an increase in the "out" scattering.

5.3 Energy Deposition in Matter

One means of identifying particles is through their energy deposition in the scintillators through which they pass. This is because the rate of energy deposition is determined by both the mass and speed of the particle.

For heavy particles (muons and pions), the energy loss is dominated by ionization of electrons in the material. The rate of energy loss is given by the Bethe-Bloche formula:

$$-\frac{dE}{dx} \approx C_0 \frac{\ln C_1 m_e \gamma^2 \beta^2}{\beta^2} - C_2 \tag{5.1}$$

where $\beta = \frac{v}{c}$, $\gamma = (1-\beta^2)^{-\frac{1}{2}}$, m_e is the mass of the electron, and C_0, C_1, and C_2 are constants determined by the material. [17]

For light particles (electrons and positrons) , the energy loss is due primarily to Bremsstrahlung. The rate of energy loss is described by:

$$-\frac{dE}{dx} \approx (\gamma - 1) m_e B_0 \tag{5.2}$$

where B_0 is a constant determined by the material. [17]

Chapter 6

Procedure for Scattering Study

The setup used for the scattering study is simply the normal PiENu apparatus with a few key differences, as illustrated in 6.1. The first difference between the PiENu apparatus and setup used for the Scattering Study was the absence of some components. During the August 2007 Scattering Study beamtest, neither the CsI array nor wire chambers 2 or 3 were installed. In addition, the BINA crystal was not yet installed, and an older TINA crystal was used in its place.

The second difference between the scattering study setup and the true PiENu setup was the introduction of a "dummy" acrylic piece between T1 and T2. This piece was always in the same location; however, its thickness was varied in 1/8" increments from 0" to 1/2". Acrylic was used because it most closely mimics the composition of the scintillating counters. Thus, by varying the width of the insert, dependence of the scattering on the thickness and number of scintillating counters can be determined.

The $\pi \rightarrow \mu \rightarrow e$ decay chain is used as the source of positrons for the scattering study. The primary reason for this choice is the vast number of $\pi \rightarrow \mu \rightarrow e$ decays. This provides excellent statistics in a much shorter time period, due to the factor of 10000 in the event rate. The second reason is the continuous energy spectrum associated with the positrons from $\pi \rightarrow \mu \rightarrow e$ decays. The $\mu \rightarrow e\nu\nu$ decay is a three body decay whereas $\pi \rightarrow e\nu$ is only a two body decay. Thus, conservation of energy and momentum require that all $\pi \rightarrow e\nu$ positrons have a fixed energy, whereas $\mu \rightarrow e\nu\nu$ positrons can take a continuous range of energies. This allows the scattering study to probe the energy dependence of the in/out scattering by observing distortions in the energy distributions in the different counters.

The last variable to be tested in the scattering study is the angular dependence of the scattering. This is accomplished by using three different acceptance conditions. These are T2, T2&T4, and T2&!T4. Referring to Figure 6.1, we can see that these three conditions describe different solid angles. Thus, by determining the change in all three acceptances as the plexiglass insert is varied, the angular dependence of the scattering can be determined.

6.1 Setup

Figure 6.1 shows the setup for the scattering study beamtest. The relative locations and sizes of the various scintillator are given in table 6.1. In addition to the scintillators there is also one wire chamber directly before the B1 counter, although it was not used in this analysis.

The scintillators are all read by photomultiplier (PM) tubes. Each scintillator is read by one PM tube, with the exception of the target and the TINA crystal. The target is read by two PM tubes (TA1 and TA2) and TINA is read by seven. The PM tubes are sampled with a 500MHz digitizer to produce a waveform, and the total charge in each PM is also integrated with an ADC.

In order to extract information about the times at which the particle passed through the various counters, each PM tube is also read with a TDC. This provides a high resolution (62.5ps) measurement of the hit times, allowing one to track the passage of the particle through the setup temporally.

Detector	Size(X)	Size(Y)	Radius(R)	Thickness(Z)	Position(Zpos)
B1	10 cm	10 cm		0.635 cm	-2 cm
B2	3.5cm	2.5 cm		0.3175 cm	-1 cm
Target	4 cm	3 cm		0.9525 cm	0 cm
T1	4.5 cm	3.5 cm		0.3175 cm	1 cm
T2			7 cm	0.635 cm	3 cm
T3	40 cm	45 cm		0.635 cm	7 cm
T4			6.35 cm	0.159 cm	9 cm
NaI			23 cm	51 cm	35 cm

Table 6.1: Locations and sizes of the scintillators. [2]

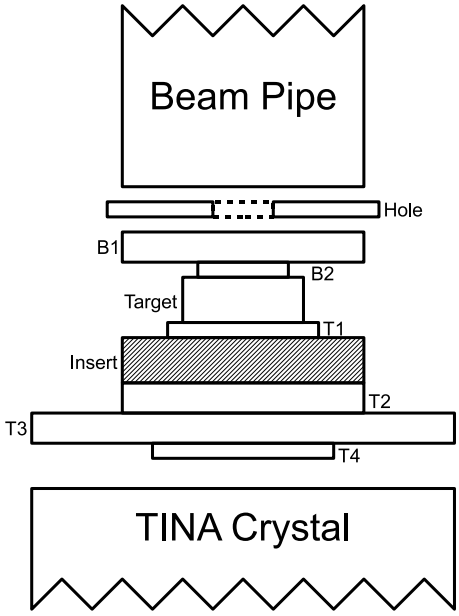

Figure 6.1: A schematic of the geometry for the August 2007 scattering study. This schematic is not to scale, but shows the approximate relative sizes and locations of the scintillators. [4]

Chapter 7

The Data

7.1 Raw Data

The data for the scattering study consists of roughly four days of beamtime during August 2007. Due to various hardware problems, there are several 'gaps' in the data; however, much of the four days produced useable data. The data is divided between the five setup configurations, corresponding to different thicknesses of plexiglass. The conditions were alternated regularly, to ensure consistency in the data. The two configurations corresponding to no plexiglass and 3/8" of plexiglass were favoured and have a much larger quantity of data. Table 7.1 outlines the approximate number of events for each of the conditions. The run numbers are used to identify the runs, and were defined at the time of the data acquisition. They increase in time and the August 2007 beamtest spans runs 1431-1931, with gaps due to data acquisition problems.

Plexiglass Thickness	Number of Events (M)
0"	80
1/8"	12
1/4"	10
3/8"	67
1/2"	35

Table 7.1: Quantity of data for the different configurations.

7.2 Variables and Definitions

For the August beamtest the trigger was defined by:

$$\mathrm{B1} \cap \mathrm{B2} \cap (\mathrm{TA1} \cup \mathrm{TA2}) \cap \mathrm{T1}$$

This ensures that no bias is introduced to the sample by including any component downstream of T1, while preferentially selecting 'downstream exiting' positrons to improve statistics.

The trigger gate was defined to be 450ns. The gate describes the maximum time between the hit in B1 that signaled an incoming particle, and the hit in T1 that signaled the outgoing particle. A successful trigger is referred to as an event.

As mentioned previously, the PM waveforms were sampled in three different ways. First, ADC's were used to integrate the waveform over two windows to produce the ADC (35ns gate) and ADCw (350ns gate) variables. Second, multi-hit TDC's were used to record the times of the pulses observed in the scintillator, to a maximum of 12 entries. Finally, a 500MHz digitizer was

used to produce a waveform from the PM signal. All of this was done for each PM tube, so this data is available for each scintillator.

After the data was acquired, the waveform was analyzed to produce several useful variables. A hit was defined by a positive peak greater than 20mV, and a NHit variable containing the number of hits in the waveform in a particular scintillator was created. In addition, each hit was indexed (to a maximum of five hits), and the time and pulse height (PH) of the peak, as well as the integrals over various windows were recorded for each hit. The windows over which the waveform was integrated are shown in Table 7.2. The start and stop times are given relative to the time of the peak.

Variable Name	Gate Start (ns)	Gate End (ns)
Q	-20	20
Qw	-20	80
Qww	-80	20
Qwp	-20	400

Table 7.2: The windows over which the waveform was integrated to generate the WF variables. The start and stop times are with respect to the pulse peak time. [3]

7.2.1 Notation

When describing a variable, the following notation is used: the detector name comes first, the type of variable comes second, the variable comes third, and an (optional) index comes last.

The detector names are B1, B2, TA1, TA2, T1, T2, T3, T4, TINASum. Where TA1 refers to the first target PM, TA2 the second target PM, TINASum the analog sum of all the TINA PM's, and the rest refer to the detectors having the same names.

The variable types are WF (the digitized waveform on the interval [-900ns,900ns] where 0 is the trigger time), WFPre (the digitized waveform on the interval [-6600ns,-900ns] where 0 is the trigger time), TDC (the multihit TDC), ADC (the short-gate (35ns) ADC integral), and ADCw (the long-gate (350ns) ADC integral).

For the WF and WFPre, the variables are: NHit, t[i] (time of i'th hit), PH[i] (pulse height of i'th hit), Q[i], Qw[i], Qww[i], and Qwp[i]. Where $i = 0, 1, ..., NHit - 1 < 5$, and the Q variables are defined above. For the TDC the variables are N (number of hits) and t[i] (time of i'th hit). Where $i = 0, 1, ..., N - 1 < 12$.

For example a variable would be something of the form B1.WF.Q[0], TA1.ADCw, T1.TDC.t[6], T3.WFPre.NHit, etc.

Chapter 8

ANALYSIS

8.1 Introduction

The ultimate goal of this analysis is the computation of the acceptances for the different hit-requirement conditions for each of the physical configurations. To accomplish this, several steps must be taken:

1. Quality control of the raw data.
2. Apply selection criteria to produce a 'pure' positron sample.
3. Verify that the sample is 'clean' to the desired degree.
4. Ensure that there is no bias in the selection criteria, nor in the definitions of variables.
5. Compute acceptances.

Run 1703 was used as the "base" run for this analysis. This is a typical run with no insert and similar beam characteristics to most of the rest of the data. Many other runs in different conditions and different data sets were also checked for consistency. The images in this report are based on the statistics of runs 1703-1712, unless noted otherwise.

Within this report, all cuts are applied in a cumulative manner, unless specified otherwise. This applies for both the figures and the fractional reductions in statistics. The reductions in statistics are expressed as the ratio of the number of events immediately after a cut to the number of events immediately before a cut.

8.2 Quality Control

The quality control of the data is a preliminary check to ensure that all hardware was functioning properly, all variables are present, and all experimental conditions were the same between runs.

8.2.1 Problems with Data

RF Signal The first problem with the data is the absence of the radio frequency (RF) timing signal from the cyclotron in the later runs. This signal provides the start time for the time of flight (TOF) from the cyclotron to the PiENu apparatus. The signal is present for roughly the first 1/3 of the runs (to run 1619), after which it disappears due to hardware problems.

T Counter ADC's The telescope counter ADC's showed time dependence, which should not exist. In particular, a malfunction in the ADC's near the end of the trigger gates produced erroneously low values. Only the first few runs (1431-1437) were functioning properly. The cause of this error is not known, but the ADC values should be treated with caution as a result.

Beam Momentum At two points during the August 2007 beamtest the B2 magnet was adjusted. After run 1437 it was lowered by $\sim 2\%$ to reduce the number of positrons in the beam. Before run 1796 the magnet was increased back to its nominal value. Table 8.1 shows that the change in the magnet strength was effective in reducing the number of positrons in the beam; however, it also decreased the momentum of the beam which is reflected in the increased energy deposition in the B counters. This change in momentum was small; however, even a small change in momentum has large effects on the acceptances because it changes the stopping location of the pions in the target. In addition, it poses problems when using the B1 and B2 energies in cut definitions. For these reasons, the 1796-1859 and 1860-1931 sets can only be compared to each other, and the 1431-1437 set must be disregarded altogether.

T1 Waveform The final anomaly observed in the data is an error in the integration of the waveform to produce the Q, Qw, and Qww variables in T1. For approximately 1% of the events in T1 the ratio $T1.WF.Q[0]/TA.WF.Qww[0] > 1$. This should never be the case, as the Q integration window is contained in the Qww integration window. This indicates that the waveform must be negative somewhere in the Qww window, bringing the reliability of both the charge (Q,Qw,Qww) variables and the hit definitions into question.

Garbage Data Due to hardware problems, some of the data acquired was either garbage or corrupt. Thus, the following runs should be disregarded, even though they fall within a set of otherwise good runs. 1557-1558, 1671, 1851, and 1883-1884.

8.2.2 Beam Properties

During the August beamtest, the B1 threshold for the Trigger was set sufficiently high that most muons and positrons in the beam were not able to produce triggers. While this is beneficial for statistics, it creates a large difference between the observed and actual beam compositions. For this reason, the hits in the pre-waveform were used to estimate the beam composition. A cut was applied to ensure that there were at least one hit in each of B1 and B2 in the pre-waveform (not exactly one, to avoid biasing against pions which produce decay products in the target), and then the type of the first particle was considered. The pre-waveform was used to eliminate bias due to beam timing; however, even the pre-waveform beam composition is biased by the hardware pion selection in the trigger. This is because the different types of particles have different times of flight, and tend to arrive "in order", even in the pre-waveform. Finally, only the type for the first particle was considered, to avoid accidentally observing target decay products.

In order to measure the beam composition, cuts were applied to select for each of the spots corresponding to positrons, muons, and pions. These cuts are shown in figure 8.1.

The beam composition for the different sets of runs in the August beamtest are shown in table 8.1. One can see that the composition is fairly consistent for most of the runs; however, the early

and late runs show an anomalously high fraction of positrons in the beam. This is due to slight differences in the magnet setting in the PiENu beamline (B2 magnetic field is slightly higher for runs 1431-1437, 1796-1859, and 1860-1931). Table 8.1 also show the mean energy of the pion spot over the August beamtest. Again, it is reasonably consistent, except for the very early and late runs, which is again explained by the different B2 magnetic field. The number of hits in the pre-waveform provides an estimate of the beam current. Once can see that it varies erratically throughout the data set. One final note on table 8.1, is that the plexiglass thickness is varied regularly throughout the beamtest. This removes the possibility that changes in acceptance were actually due to beam properties varying with time.

Start	Stop	Insert	e^+	μ^+	π^+	B1.Qw	B2.Qw	# Pre-Hits
1431	1437	3/8	0.24	0.25	0.51	1005	2247	1082692
1472	1483	3/8	0.10	0.28	0.62	1099	2339	727657
1517	1562	0	0.09	0.27	0.64	1107	2340	698340
1563	1586	1/8	0.10	0.27	0.63	1112	2339	718463
1587	1607	1/4	0.10	0.28	0.62	1115	2340	727589
1608	1621	3/8	0.09	0.29	0.61	1119	2328	1184209
1622	1640	0	0.09	0.28	0.63	1118	2330	788820
1641	1659	3/8	0.09	0.29	0.62	1120	2327	1041198
1660	1682	0	0.09	0.27	0.63	1123	2330	847745
1683	1702	3/8	0.10	0.29	0.61	1125	2334	705563
1703	1712	0	0.10	0.28	0.63	1126	2333	681485
1713	1781	1/2	0.10	0.29	0.61	1126	2322	742808
1796	1859	3/8	0.19	0.30	0.51	1115	2193	988647
1860	1931	0	0.21	0.29	0.50	1112	2178	1040873

Table 8.1: Summary of the data from the August 2007 beamtest. Start indicates the first run number, stop indicates the last run number, and insert indicates the condition of the set of runs. The beam components (positrons, muons, and pions) are expressed as normalized percentages. The B1 and B2 energies were determined from the mean of the distribution of the pion spot. Pre-hits refers to the number of events in WFPre, given approximately the same number of events in the WF.

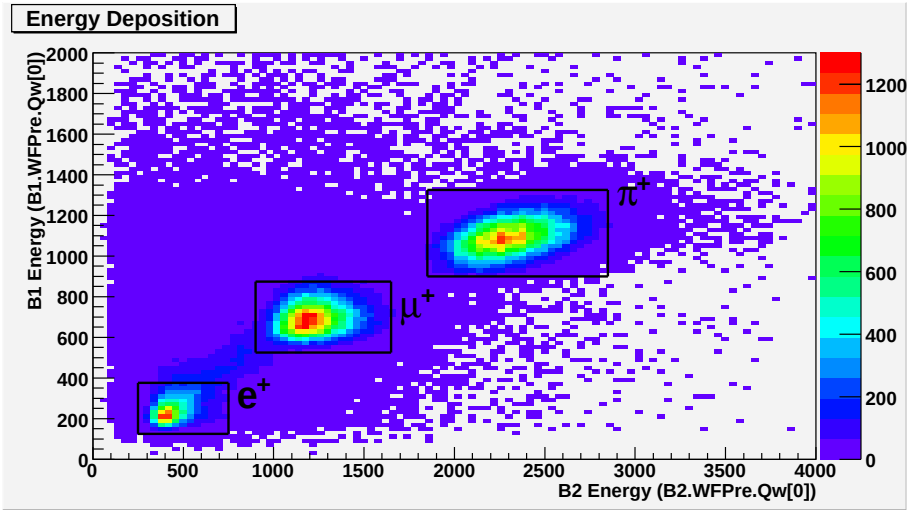

Figure 8.1: Plot of the B1 and B2 energies. The Qw variable extracted from the pre-waveform was used for the B1 and B2 energies. The boxes show the cuts for the e^+, μ^+, and π^+.

8.3 Selection Criteria

8.3.1 Pileup

The first basic cut is a pileup cut. Pileup refers to coincidence events, in which either two pions enter or two decays in the target occur within one trigger gate. This causes problems because an analog addition occurs in the waveform of the PM tubes giving falsely high energy measurements for both particles. Due to the fact that the particles' energies are used in identification, it is important that these particles be disregarded. A pileup cut excludes events of this type by requiring that only one pulse was observed in each waveform. A pileup cut cannot be applied to every waveform, as excluding pileup in T2 and T4 would bias their acceptances to lower values. That said, due to the geometry of the detectors, a restriction on T1 is sufficient.

This is accomplished by requiring that only one hit is observed in each of the B counters, one hit in T1, and fewer than four hits in the Target (because both $\pi \rightarrow e$ and $\pi \rightarrow \mu \rightarrow e$ events have at most three). In addition, the Hole variable is used as a veto, to ensure that no stray particles entered the setup at large angles.

The pileup cut is defined by:

$$\text{B1.WF.NHit} == 1 \cap \text{B2.WF.NHit} == 1 \cap \text{T1.WF.NHit} == 1 \cap$$
$$\text{TA1.WF.NHit} < 4 \cap \text{TA2.WF.NHit} < 4 \cap \text{Hole.WF.NHit} == 0$$

This cut is shown in figure 8.2. It produces a major reduction in statistics to 56%, which is unfortunate, but obviously necessary.

As mentioned in the Procedure section, the rate of incoming pions was chosen to maximize statistics. It is a compromise between maximizing the event rate and minimizing pileup. Thus, although decreasing the event rate would decrease the loss of statistics to pileup, it would involve a loss of statistics in the raw data producing a net loss of statistics in the end.

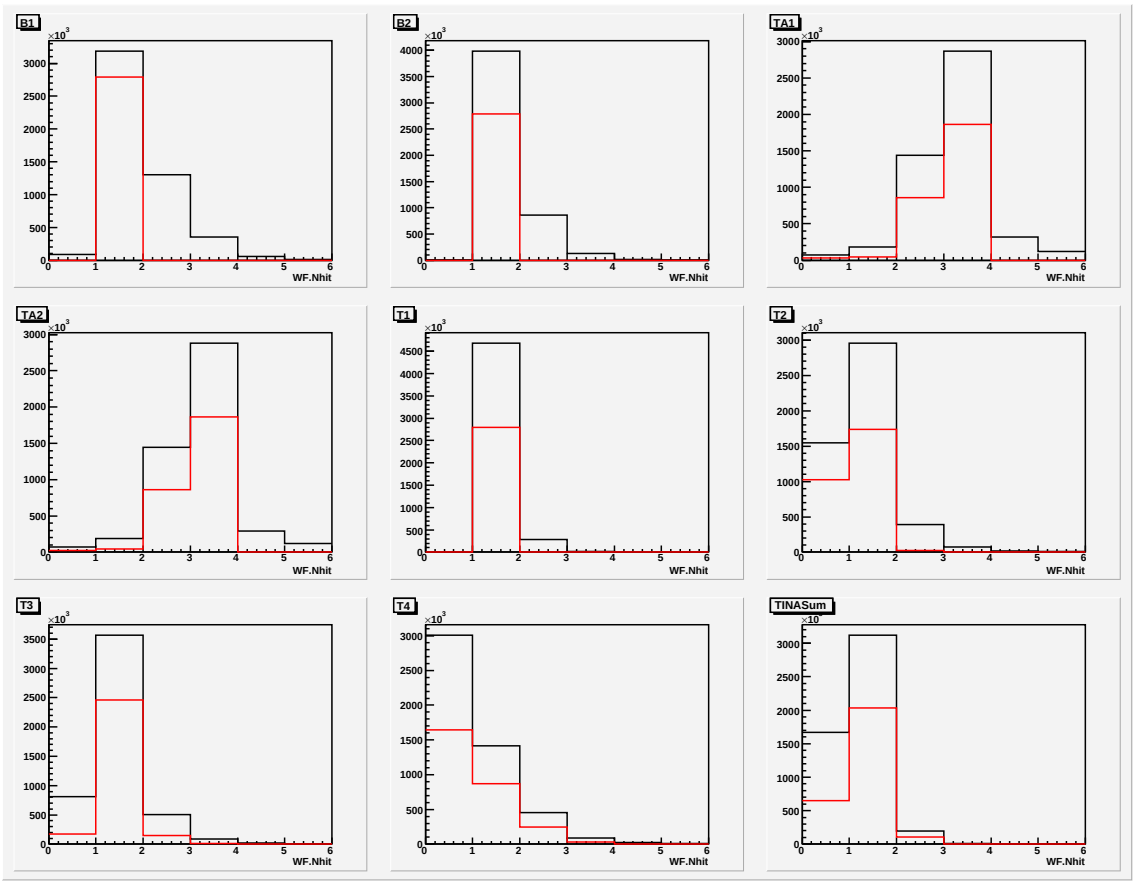

Figure 8.2: Plot showing the number of hits in the various detectors before (black) and after (red) the pileup cut.

8.3.2 Prepileup

The second basic cut is a prepileup cut. Prepileup is analogous to pileup in that we would like only one hit in most of the waveforms. The difference, is that we are requiring that the waveform be clear immediately before a signal of interest. This is to ensure that there are no pileup effects, and that the observed decays and hits all correspond to the particle we are interested in or its decay products. The prepileup requires that all of the PM waveforms for all of the scintillators were clear for $6.6\mu s$ before the particle of interest entered. It is not strictly necessary to include the Target waveforms in this cut, as a pre-hit in the target may not correspond to an extra particle at all; however, they provide only a slight decrease in statistics, so they were included for consistency. Also, the pileup cut is used primarily to suppress background in the T1-B1 time distribution which is a neutral bias with respect to the thickness of the insert. Thus, the pileup cut could be relaxed (by requiring that only the $300ns$ immediately before the particle of interest were clear); however, statistics are not a major concern in this analysis so the full cut was used.

The prepileup cut is defined by:

$$\text{B1.WFPre.NHit=0} \cap \text{B2.WFPre.NHit=0} \cap \text{TA1.WFPre.NHit=0} \cap \text{TA2.WFPre.NHit=0} \cap \text{T1.WFPre.NHit=0} \cap \text{T2.WFPre.NHit=0} \cap \text{T3.WFPre.NHit=0} \cap \text{T4.WFPre.NHit=0}$$

This cut is shown in figure 8.3. This cut results in a reduction in statistics to 30%, which is, again, very large but necessary.

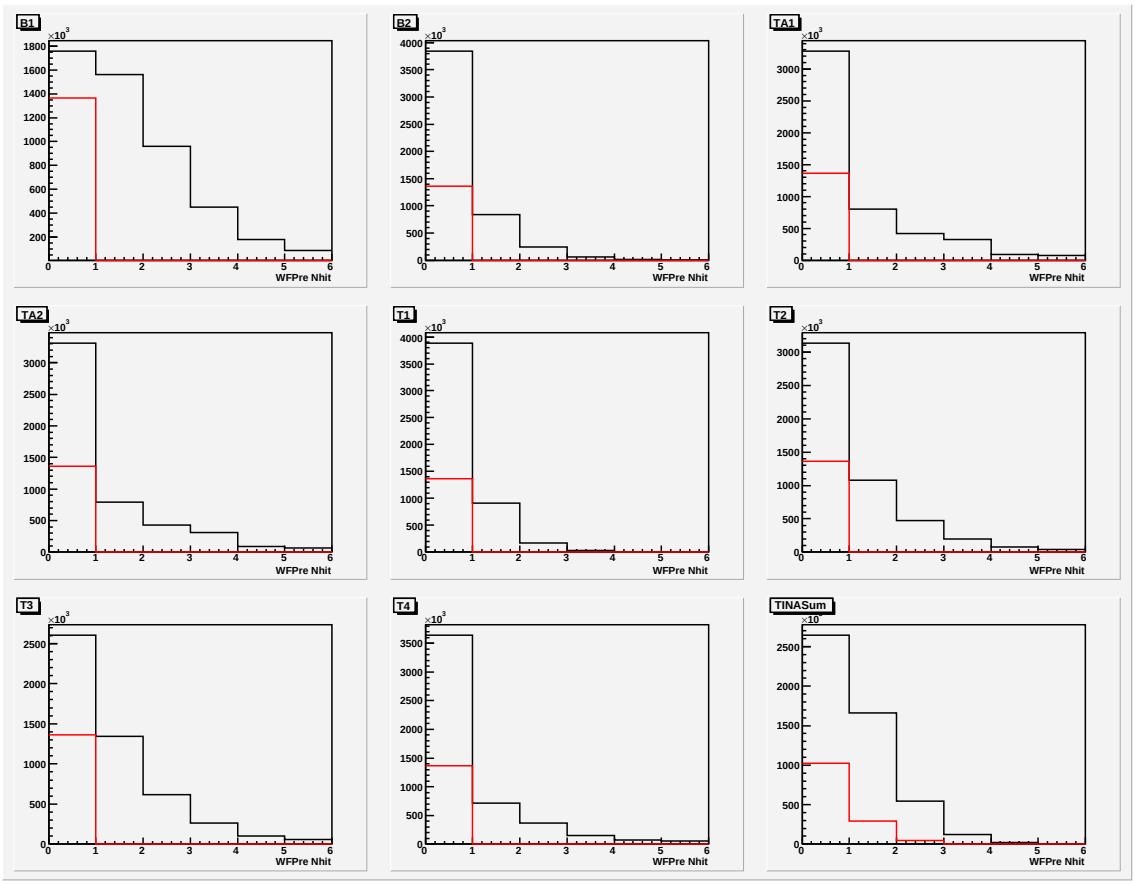

Figure 8.3: Plot showing the number of WFPre hits in the various detectors. The data before the prepileup cut is shown in black and the data after the cut is shown in red.

8.3.3 Pion Selection

The pion beam is contaminated with many types of particles. These include muons and positrons produced from decays in flight, and neutral particles and protons produced by interactions of the beam with nuclei. The purpose of pion selection is to eliminate these other contaminants to produce a pure sample of pions in the target. Typically, both the time of flight of the particles from the cyclotron and the energy deposition in the counters are used to identify pions. As noted in the Quality Control section, there was a technical problem with the timing signal from the cyclotron in most of the August beamtest runs, making TOF identification impossible. For this reason, only particle energies were used for identification.

Particle identification through energy deposition is made possible through the selection of a specific beam momentum by the PiENu beamline. Since all particles have the same momentum and the masses of the different constituents are not the same, it follows that their speeds must also differ. As mentioned in the Theory section, the amount of energy deposited per unit length in a material depends on both the type of particle and the speed. Thus, the different types of particles each deposit a different amount of energy in each of the B counters.

The energy cut accepts only a narrow range of energies in the B1 and B2 detectors, corresponding to the characteristic energy deposition of pions. The energy cut is defined as:

$$900<\text{B1.WF.Qw[0]} \cap \text{B1.WF.Qw[0]}<1300 \cap 1700<\text{B2.WF.Qw[0]} \cap \text{B2.WF.Qw[0]}<2900$$

This cut is indicated by the box in Figure 8.4. There are a few noteworthy features in this image. First, there is a clear horizontal cutoff line at ~ 900 corresponding to the thresholds of B1. This cutoff is higher than the typical energy deposited by a positron or a muon, providing an immediate hardware cut that prevents incoming muons and positrons from producing triggers. Second, there is a spot due to two-hit events which escaped the pileup cut, which is effectively dealt with by the energy cut.

Due to the fact that the threshold values already exclude most muons and positrons, the energy cut only produces a slight reduction in statistics to 96.5%. Setting these thresholds as close as possible to the pion spot maximizes the fraction of triggers that are not subsequently removed by software cuts.

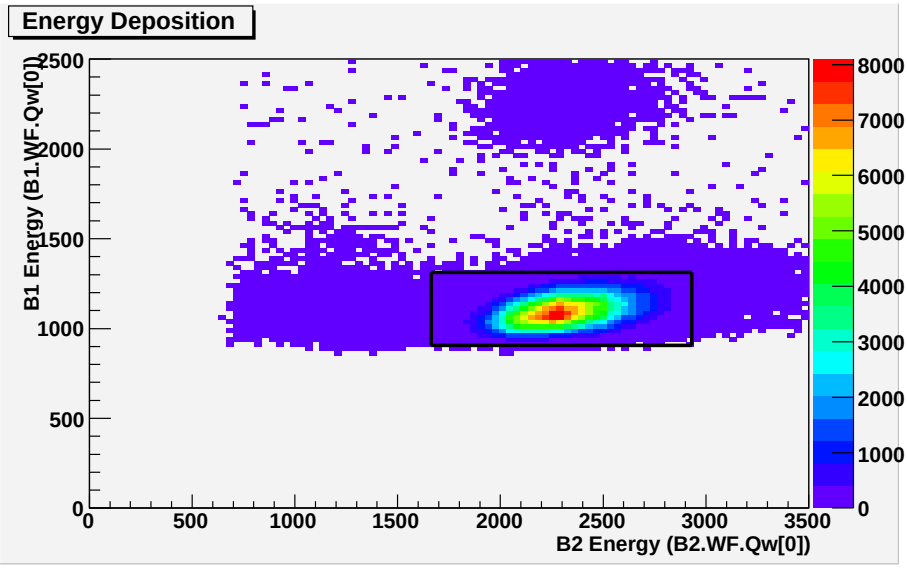

Figure 8.4: A plot of the energy deposited in B1 vs. the energy deposited in B2. This plot includes only the values for the first hits in B1 and B2 and shows the data after the pileup and prepileup cuts have been applied. The box denoted the selection of the energy cut.

8.3.4 Summary of Basic Cuts

The effects of the three basic cuts are shown in figure 8.5. The black line denotes the raw data, the red the pileup cut, the blue the pre-pileup cut, and the green the pion-energy cut; where all cuts are applied cumulatively. We can see that the pileup cut provides a strong background suppression, eliminating many early and late hits, as well as an elimination of the periodic background due to the 43ns cyclotron pulses. The effects of the pre-pileup cut are less obvious; however, it too provides a suppression of the background. Finally, we can see the effect of the energy cut. This cut provides only a slight reduction in most of the spectrum; however, it provides a large cut at early times due to a reduction in fly-through muons.

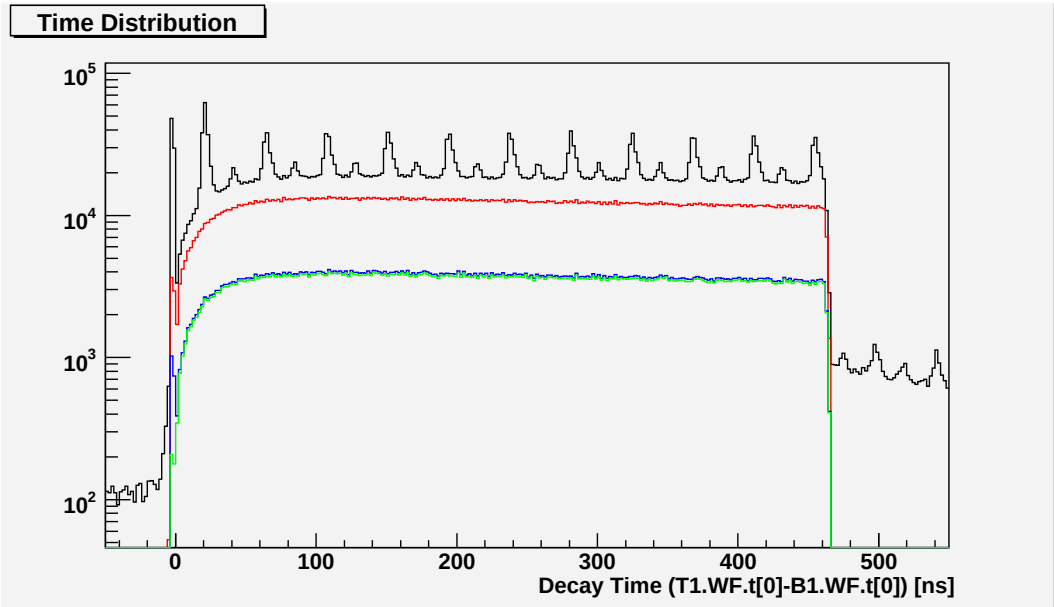

Figure 8.5: This image shows the result of the basic cuts on the decay time (T1-B1) distribution. The uncut data is black, the pileup cut is red, the prepileup cut is blue, and the energy cut is green.

8.3.5 Muon decays in T4

As mentioned in the previous section, muons in the beam typically stop in the T4 counter. The trigger thresholds were defined such that most muons do not cause a trigger and are, therefore, not recorded as events. This greatly reduces the problem of false events due to muon flythroughs; however, it neglects a second problem, that is the accumulation on muons in T4. This is particularly problematic as the acceptance of the T4 counter is crucial to this analysis, and muon decays in T4 will cause the T4 acceptance to be falsely high. An immediate response would be to eliminate T4 pileup by requiring only one T4 hit; however, this selectively eliminates events in which a true target-produced positron was seen in T4, as well as a signal due to a muon decay in T4. This would bias the T4 acceptance making it falsely low, so these events should be kept. The aim is therefore to exclude events in T4 where one or more hits were observed; however, *none* of these corresponded to a target-produced positron.

A first step is a purely geometric restriction. Referring to table 6.1, we can see that the T3 counter if significantly larger than the T4 counter. In particular, the T4 counter is completely 'hidden' behind the T3 counter, as viewed from the target. For this reason, any event in T4 must have also been seen in T3.

Thus, we define a T4 pileup cut by:

$$\text{T3.WF.NHit} > 0 \cup \text{T4.WF.NHit} = 0$$

This cut provides a reduction in statistics to 99.7%.

8.3.6 Positron Timing

The second method of eliminating spurious events in T4 due to local muons decays is to implement a timing restriction, requiring a coincidence between T4 and T1. In fact, this technique is useful for T2 and T3 as well. All discussion will be based on T4-T1 coincidence; however, the same is true for T2-T1 coincidence and T3-T1 coincidence.

In order to implement this cut, it would be ideal to define a time coincidence based on the TDC data because of the improved time resolution. For the August beamtest; however, the threshold on the TDC was set to a minimum in order to minimize distortion in time measurements due to the pulse shape. Thus, there are many TDC hits, most of which are noise, making it very difficult to identify which TDC hit corresponds to the positron.

The pileup cut requires exactly one hit in T1. Thus, the T1.WF.t[0] variable provides the reference time against which all other hit times can be measured.

To avoid biasing the sample, we cannot require that every hit in T4 be a coincidence with T1.WF.t[0], as this would discard events where a coincidence event occurred and a subsequent decay in T4 occurred some time later–falsely lowering the acceptance of T4. Instead we must require that either no hits were seen in T4, or one of the hits was a coincidence.

The implementation of this cut in ROOT is long-winded and messy, but the definition is:

$$\begin{aligned}&(\text{T2.WF.NHit} = 0 \cup \exists i \text{ s.t. } |\text{T2.WF.t[i] - T1.WF.t[0] - } a_2| < b_2) \cap \\ &(\text{T3.WF.NHit} = 0 \cup \exists i \text{ s.t. } |\text{T3.WF.t[i] - T1.WF.t[0] - } a_3| < b_3) \cap \\ &(\text{T4.WF.NHit} = 0 \cup \exists i \text{ s.t. } |\text{T4.WF.t[i] - T1.WF.t[0] - } a_4| < b_4)\end{aligned}$$

where the a's and b's are constants describing the location and width of the peaks. The locations of the peaks were found to be [0,16], [-6,16], and [-20,20] for T2, T3, and T4, respectively. This gives (a_i, b_i) values of (8,8), (6,10), and (0,20) for the three counters.

The effect of this cut is shown in figure 8.6. The plotted quantity is the $\min_i$|T2.WF.t[i] - T1.WF.t[0]|. We can see that this cut is effective, as it completely removes the background away from the peak. There is obviously still some background hidden under the peak; however, we have achieved suppression by a factor of ~ 40. This cut provides a reduction in statistics to 99.8%.

One final note on figure 8.6, is the skew nature in the T4 plot. This is due to the dependence of the T4 time on the pulse shape, causing a slight distortion to larger times for larger pulses.

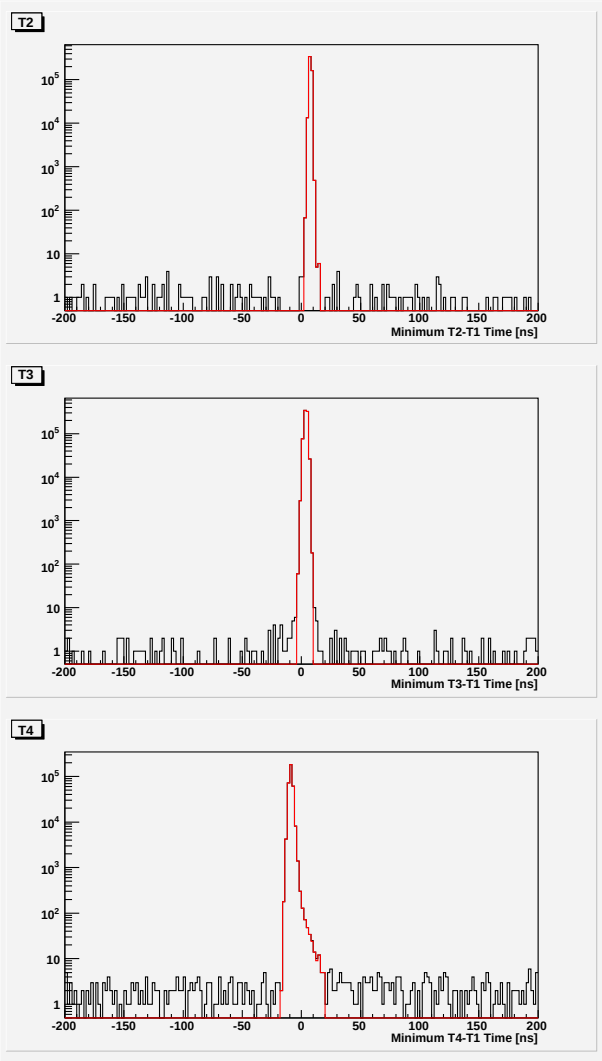

Figure 8.6: This image shows the minimum time between the only hit in T1 and any hit in T2 (top), T3 (middle), and T4 (bottom). The black line denotes the data before the timing coincidence cut, and the red the data after the cut.

8.3.7 Other Contamination

As mentioned previously, there is also contamination of the beam by neutral particles and protons. The neutral particles will not interact with the counters (only the TINA crystal), and we are only concerned with the acceptances of the T2 and T4 counters so they can be ignored in this analysis, as they will contribute to neither the positron sample nor the hits in the counters.

Protons are, in general, traveling so slowly that they rarely pass beyond B2 or even B1. Thus, they are unable to produce triggers, and have no bearing on the T counters. Thus, they are not considered in this analysis as they have no bearing on the T2 or T4 acceptances.

8.3.8 Summary of Cuts

Table 8.2 shows the reduction in statistics resulting from the application of the cuts (sequentially). The overall effect is a reduction to only 16% of the raw statistics; however, the quantity of data is large enough that the statistics will be sufficient to test the simulation.

Cut	Reduction	Events Remaining	Percent Remaining
None	1.000	4997190	1.0000
Basic Pileup	0.559	2792825	0.5589
Prepileup	0.302	842758	0.1686
Energy	0.965	813120	0.1627
T4 Muon Pileup	0.997	811019	0.1623
Positron Time	0.998	809060	0.1619

Table 8.2: Table showing the effects of the cuts. The Reduction refers to the change in statistics, Events Remaining refers to the sample size after the cut, and the percent remaining refers to the fraction of the total sample remaining after the cut.

8.4 Checking Cuts

8.4.1 Time of Flight Check

As explained in the Energy Cut section, the common momenta and differing masses of the particles in the beam cause their speeds to differ. As a result, if the particles travel a large distance, such as that from the graphite target to the PiENu setup, their travel times will differ significantly. This provides an excellent means to identify particles for pion selection. Unfortunately, the signal for the reference time from the cyclotron was not available for many runs, so the TOF cannot be used in selection. That said, the runs for which TOF selection is possible can still be used to test the effectiveness of the energy cut.

Figure 8.7 shows the TOF distribution of the uncut data on the top, as well as the sample after the pileup, prepileup, and energy cuts on the bottom. The cyclotron reference signal is not available for runs 1703-1712, so runs 1517-1537 have been used to produce this figure. Comparing the two histograms, it is immediately obvious that the cuts designed to eliminate pileup and select pions are both effective and sufficient. The bottom figure shows almost no background outside

of the pion spots separated by the characteristic 43ns pulses from the TRIUMF cyclotron. The remaining background is on the order of 0.01%, which is an order of magnitude better than necessary.

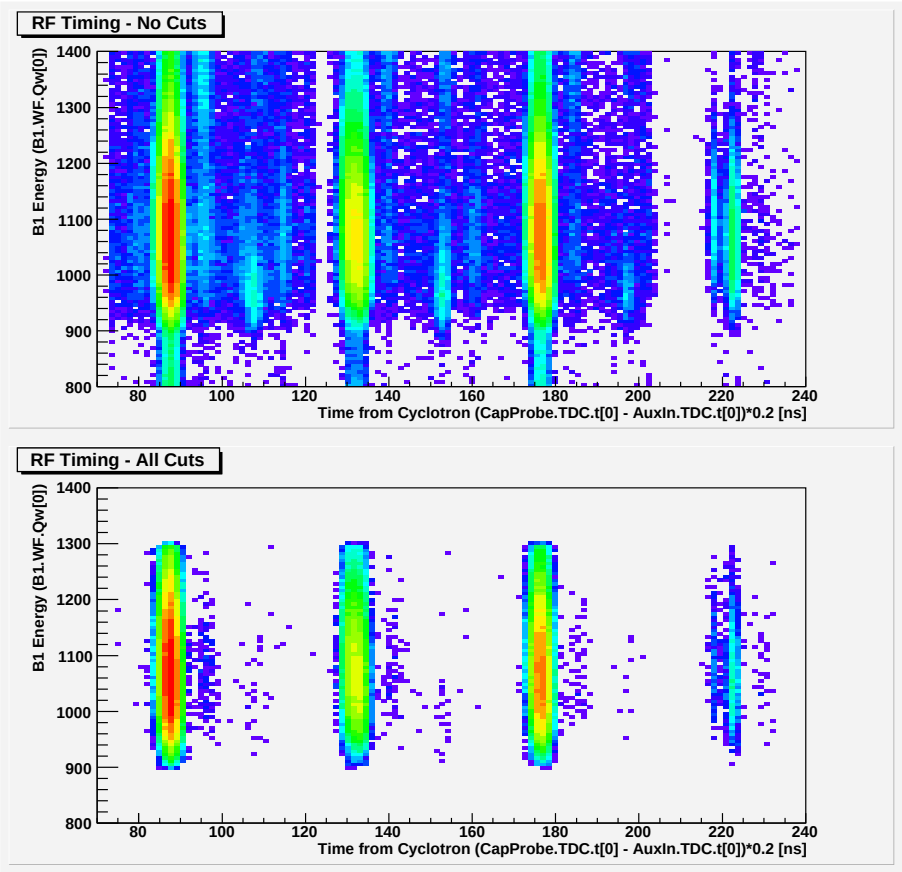

Figure 8.7: Histogram of particle energy (B1) vs. the time of flight from the cyclotron. The top image shows the data with no cuts and the bottom the data after the pileup, prepileup, and energy cuts. Runs 1517-1530 were used to produce this image, as the RF signal was not available for the the base runs.

8.4.2 Q/Qww in B counters Check

Referring to the section on the waveform variables, we can see that there were several charge variables produced by integrating over different windows. These provide an important pileup check. Any events where undetected pileup occurred should have a disagreement between these variables as the longer gates are sensitive to pileup whereas the shorter ones are not. In particular, a comparison of the Q and Qww variables for the counters used in the pileup cut provides an important verification of this cut.

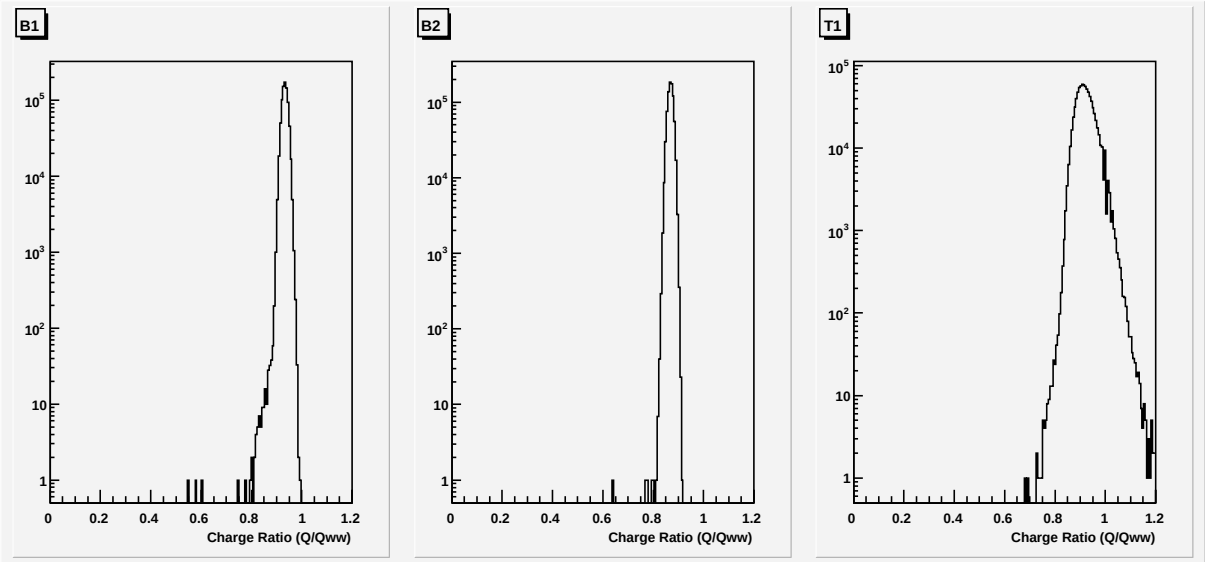

Figure 8.8: Plot of the distribution of the ratio Q/Qww for B1 (top), B2 (middle), and T1 (bottom). The data shown is after the application of the all cuts.

In figure 8.8 we can see the pileup test for the B1, B2, and T1 counters. As expected, all three plots are sharply peaked at a value slightly below 1.0. The value is lower than 1.0 due to the shape of the pulse, and the fact that the value sometimes exceeds 1.0 for the T1 plot is due to an error in the T1 waveform. The fact that there are very few events significantly below 1.0 indicates that there is essentially no pileup remaining.

8.5 Estimating Backgrounds

8.5.1 Positron Backgrounds

The most problematic source of background in determining the acceptances of T2 and T4 is the presence of dormant muon decays in T4. The muon stops are excluded by the pion selection cut; however, the increase in the T4 acceptance due subsequent decays is unavoidable. In addition, the problem worsens as the stopping location of the muons depends on the thickness of the insert, so the bias varies with the insert condition.

A timing cut his been implemented to remove events where the T1 positron and the T4 positron were not correlated in time, with great success. The only problem that remains is to

estimate the number of background events remaining that are purely coincidence events in which a positron passed through T1, and then a second unrelated positron passed through T4 within a short time period. To accomplish this we simply fit the constant background in the time spectrum (before the positron timing cut), and extrapolate it under the peak.

The fit of this off-peak background to a constant function is shown in figure 8.9. The background in T2, T3, and T4 were all fitted separately. The backgrounds were 1.2, 1.2, and 1.8 events/bin in T2, T3 and T4 respectively. Since the peaks were 8, 10, and 20 bins wide, this gives a total background of roughly 50 events in a sample of 809060, for a level of 0.006%. This is well below the requirement of 0.1%; however, we see that the positron timing cut was absolutely necessary for the factor of 40. It should be noted that these backgrounds in T2, T3, and T4 are not independent, as the same uncorrelated particle may pass through several detectors. Thus, by adding the three backgrounds together, we get a conservative upper bound on the total background.

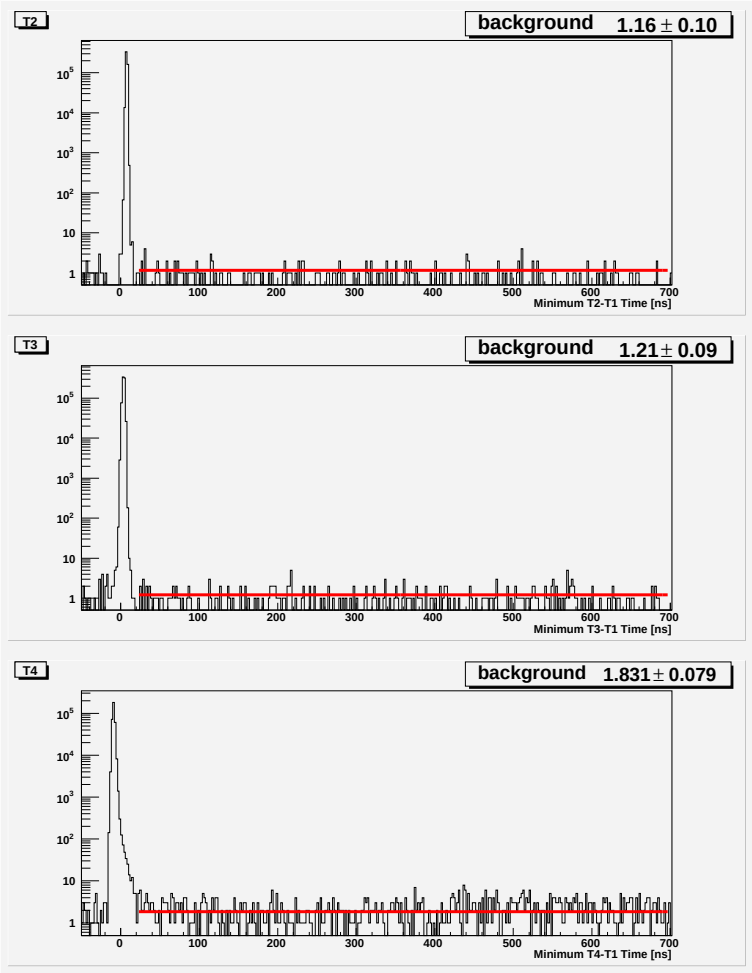

Figure 8.9: Plot of the minimum time between the only hit in T1 and any hit in T2 (top), T3 (middle), and T4 (bottom). The red line denotes the fitting (constant) function which was fit to the background away from the peak.

8.5.2 T1-B1 Timing Background

Due to the characteristic exponential decays associated with the pion and muon, the time distributions can be precisely predicted and tested with fits. In particular, the distribution of the decay time for a $\pi \to \mu \to e$ decay is given by:

$$p(t) = \int_0^t e^{-\frac{t'}{t_\pi}} e^{-\frac{t-t'}{t_\mu}} dt' = \frac{t_\pi t_\mu}{t_\mu - t_\pi} \left(e^{-\frac{t}{t_\mu}} - e^{-\frac{t}{t_\pi}} \right) \tag{8.1}$$

where t_π and t_μ denote the lifetimes of the pion and the muon respectively.

This motivates us to fit the histogram of the T1-B1 time difference with the function:

$$f(t) = p_0 + p_2 \left(e^{-\frac{t-p_1}{t_\mu}} - e^{-\frac{t-p_1}{t_\pi}} \right) \tag{8.2}$$

where p_0 is a constant background term accounting for dormant muons in the target, p_1 is a time offset determined by the hardware, and p_1 is a scaling factor determined by the quantity of data.

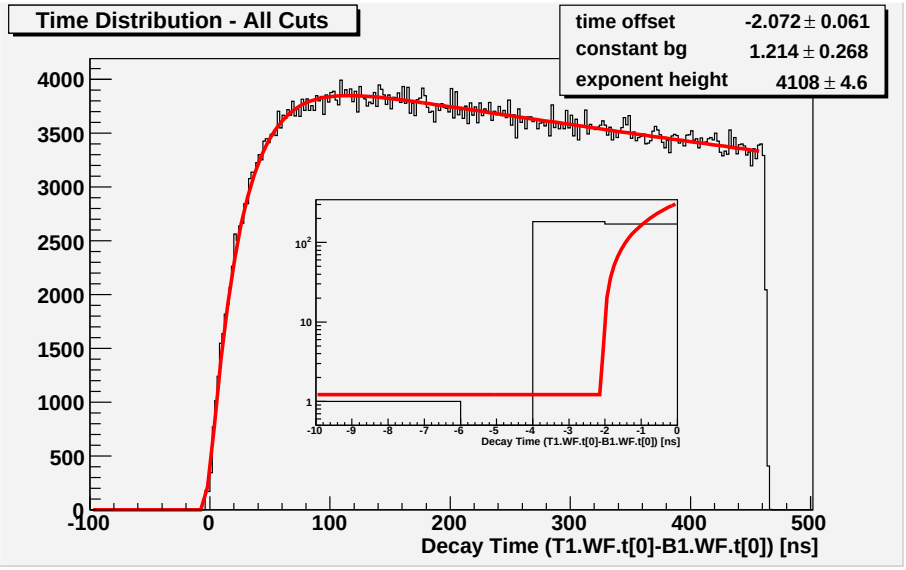

Figure 8.10: Plot of the T1-B1 time distribution fit with the model $f(t)$ for a $\pi \to \mu \to e$ decay. The insert shows the fit at small times to demonstrate the time offset, the small background, and the presence of fly-through particles.

As shown in figure 8.10, the T1-B1 time distribution is very well described by the model for $\pi \to \mu \to e$ decays. From our fitted parameters and the disagreement between the model and the data, we can determine the level of the backgrounds.

The constant background term provides a measure of the rate of decays in the target that are uncorrelated with the pion stop. This background is approximately 1.2 decays/bin, over 300 bins giving 360 events. The sample size is 809060 events, giving a background level of 0.045%. These positrons may be uncorrelated with the incoming pion, but they have the same energy and angular distributions as regular pimue positrons, so they should not bias the sample.

The largest systematic discrepancy between the model and the data occurs at small negative times. The $[-4, -2)$ bin exceeds the model by $\sim$ 180 events. These events are not explained by the model, and are presumably due to a background of muons which fly-through the target giving unreasonably low T1-B1 time differences. Since the sample size is 809060 events, we have a fly-through background level of 0.022%. The muons will fly-through T1 and T2, and come to rest in T3 or T4, depending on the thickness of the insert. Due to their higher mass, muons will tend to scatter less than positrons, so this background will bias the sample.

8.5.3 Summary of Backgrounds

The summary of the remaining backgrounds are shown in table 8.3. We can see that each of these is less than the desired 0.1% level, and even the sum including the neutral backgrounds is sufficiently small. This demonstrates that the sample meets the desired criteria, and the insert-dependent differences in the acceptances are reliable to sufficient precision.

		T2 Bias		T4 Bias	
Cause	Level (%)	0”	1/2”	0”	1/2”
Dormant Muons	0.045	N	N	N	N
Fly-Through Particles	0.022	+	+	+	-
T3/T4 Muon Decays	0.006	+	+	++	++

Table 8.3: The estimates of the remaining levels of the various backgrounds. The 0” and 1/2” denote the thickness of the insert. + denotes a positive bias, ++ a strong positive bias, - a negative bias, and N is neutral.

8.6 Checking for Bias

The final task it to check our hardware and software for any bias introduced. The apparatus and DAQ process are designed to be as neutral as possible, so this is more of a formality. The only potential introduction of bias is in the definition of a hit in the waveform.

8.6.1 PH Bias

When extracting variables from the waveform, a hit is defined as a positive peak greater than 20mv. This definition is consistent for all of the plexiglass conditions; however, there is potential for a bias due to the threshold value. Since the PH distributions in T2 and T4 may differ for the different plexiglass conditions, different fractions of low-energy or large angle positrons may be excluded by this cutoff.

This bias can be ruled out by verifying that the T2 and T4 pulse height (PH) distributions are consistent at low values for the different insert thicknesses. In figure 8.11 we can see the normalized T2 and T4 PH distributions for the the no insert (black), and 3/8” insert (red) data. We can see that the distributions agree, for the most part, except that the data with the insert tend to have a slightly larger high energy tail (presumably due to increased positron absorbtion, or an increased number of positrons at large incident angles) and a slightly suppressed low energy

region (due to the normalization). The insert shows the two nonzero bins with the lowest PH. We can see that the distributions for the two samples do disagree statistically at low PH, so some bias is present.

Estimating the differences in the distributions to be 0.0008 for T2 and 0.0005 for T4, and extrapolating over the PH<20mv region indicates that the acceptances for the sample with the 3/8" insert are biased to be high by approximately 0.08% in T2 and 0.05% in T4. The bias for the other insert conditions can be found by a linear interpolation (or extrapolation for the 1/2" case). This bias is quite small (smaller than 0.1%) but should be kept in mind when considering the final acceptances, as it will increase the apparent acceptances for the runs with thicker inserts.

There is one final noteworthy aspect of figure8.11 pertaining to the binning. The PH variable is read off from the (digitized) waveform, and is, therefore, discretized. Not only is it discretized, but the discretization is inconsistent over the distribution (the lumps are not always the same distance apart) and varies between the different runs. For this reason, a very large sample of runs and large histogram bins were used to average out any binning artifacts. The fact that the two lowest bins show the same bias provides evidence that the difference in the distributions is not due to binning (because if the first bin randomly had one extra set of data, then the second should have one fewer), but this bias should be interpreted with caution.

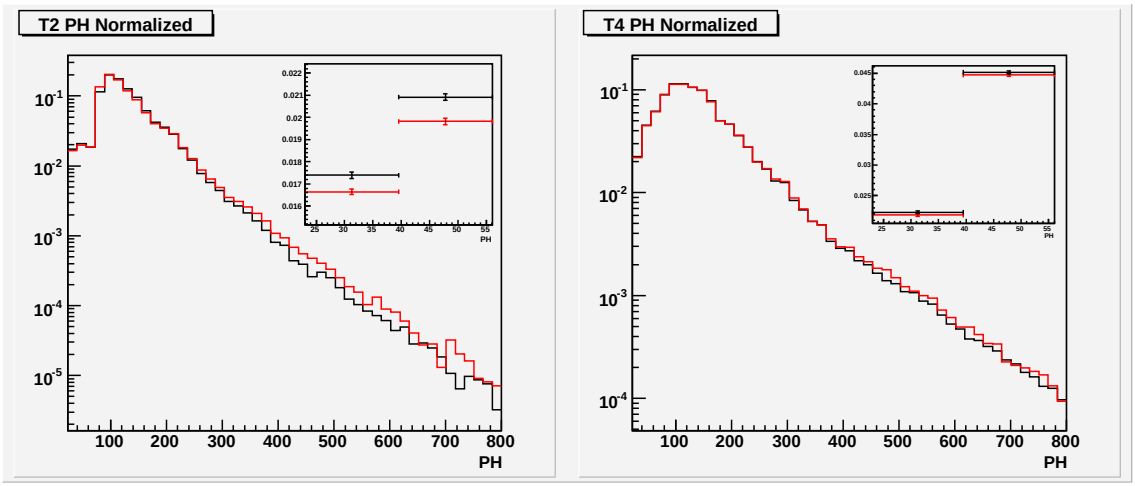

Figure 8.11: Plot of the normalized PH distributions in T2 (left) and T4 (right) for the no insert (black) and 3/8" insert (red). The insert shows the two nonzero bins with lowest PH.

Chapter 9

Final Acceptances

The final acceptances for the different sets are shown in table 9.1, and graphically in figure 9.1. There are several noteworthy features of these results.

First and foremost, the expected difference between the different conditions exists. In addition, there is a noticeable difference between the runs at different beam momentums, providing a good test of the simulation.

The next noteworthy feature is the magnitude of the statistical uncertainties, which were computed by:

$$\sigma A = A\sqrt{\frac{1}{n} - \frac{1}{N}}$$

where $A = \frac{n}{N}$ is the acceptance, n is the number of events satisfying the condition, and N is the total number of events. We can see that the uncertainties are on the order of $0.01 - 0.1\%$, making them acceptable, but only marginally. In order to reduce these uncertainties, the acceptances for the different sets with common conditions should be combined. This is not necessarily possible, as the beam properties differ between sets–bringing us to the last noteworthy point.

Start	Stop	Insert	B2 Magnet	Current	T2	T2&T4	T2&!T4
1431	1437	3/8	High	High	60.08±0.12	37.30±0.12	22.78±0.10
1472	1483	3/8	Normal	Normal	61.12±0.05	38.29±0.05	22.83±0.04
1517	1562	0	Normal	Normal	63.29±0.03	39.35±0.03	23.94±0.02
1563	1586	1/8	Normal	Normal	62.35±0.04	39.08±0.04	23.27±0.03
1587	1607	1/4	Normal	Normal	61.66±0.04	38.68±0.04	22.98±0.03
1608	1621	3/8	Normal	High	62.16±0.05	38.58±0.05	23.58±0.04
1622	1640	0	Normal	Normal	63.61±0.04	39.31±0.04	24.30±0.04
1641	1659	3/8	Normal	High	61.54±0.04	38.25±0.04	23.29±0.03
1660	1682	0	Normal	Normal	63.38±0.04	39.10±0.04	24.28±0.03
1683	1702	3/8	Normal	Normal	61.13±0.04	38.15±0.04	22.98±0.03
1703	1712	0	Normal	Normal	63.33±0.05	39.19±0.05	24.14±0.05
1713	1781	1/2	Normal	Normal	60.75±0.02	37.71±0.02	23.03±0.02
1796	1859	3/8	High	High	61.85±0.02	37.26±0.02	24.60±0.02
1860	1931	0	High	High	63.94±0.02	38.13±0.02	25.81±0.02

Table 9.1: The final acceptances for the different data sets. The start, stop, and insert values have their usual meaning, the B2 Magnet and Current describe the beam momentum selection and the cyclotron current respectively. The last three columns provide the final acceptances, with uncertainties, as percentages.

Within a given condition, the different sets show a mix of variation. The 0" data is quite consistent indicating that a) the beam properties were reasonably constant between sets, and b) the setup without the insert is mostly neutral to slight changes in the beam properties. The 3/8" data on the other hand, varies greatly between sets. From table 9.1, we can see that sets 1608-1621 and 1641-1659 have increased beam intensities as well as significantly different acceptances. It is not clear why an increased ratio of pre-pileup particle to triggers (which presumably corresponds to an increased beam intensity) would change the acceptances of wither T2 or T4.

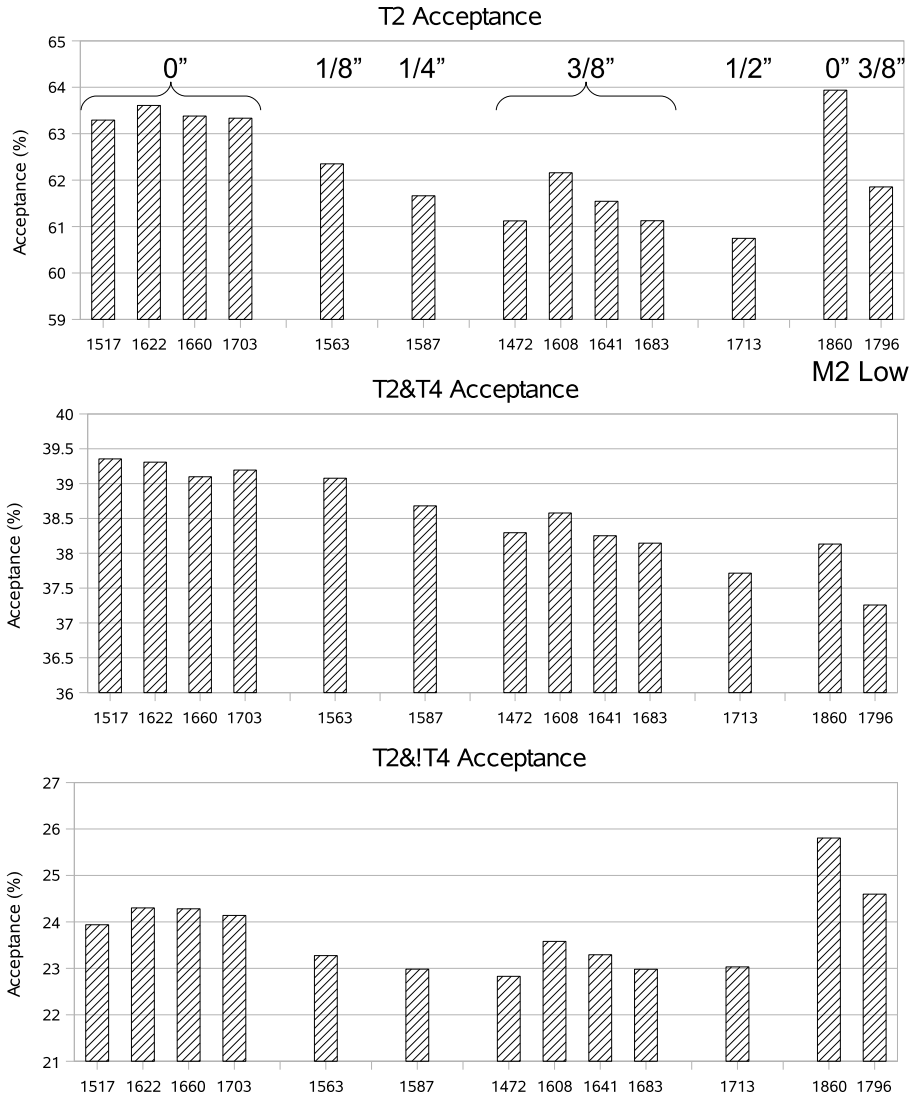

Figure 9.1: Plot of the acceptance for T2 (top), T2&T4 (middle), and T2&!T4 (bottom). The different insert conditions are shown in groups, with increasing thickness to the right. The last two columns denote the sets with a different momentum, which can only be compared to each other. The index on the x-axis denoted the run number of the start of the set. Finally, the set 1431-1437 has been excluded because it cannot be compared to any other data.

Possible explanations could include a) an increase rate of fly-through particles or b) increased number of protons produced in the target, both of which would increase the acceptances. Possible cuts to eliminate these events would include eliminating the early part of the time spectrum

T1.WF.t[0]-B1.WF.t[0] >20

and requiring that there be at least two hits in the target

TA1.WF.NHit >0 && TA2.WF.NHit >0.

These cuts were implemented to test these theories; however, there was no observed change in the acceptances. Future work is necessary to understand this dependence, as it implies that there is something unknown that was overlooked in the analysis.

Until this effect is better understood, the simplest solution is to simply exclude the 1608-1621 and 1641-1659 sets, as the other 3/8" sets had similar beam properties to the sets with other inserts. This gives final acceptances for the different conditions as shown in table 9.2.

Beam	Condition	T2	T2&T4	T2&!T4
Normal	0	63.38±0.02	39.27±0.02	24.11±0.02
	1/8	62.35±0.04	39.08±0.04	23.27±0.03
	1/4	61.66±0.04	38.68±0.04	22.98±0.03
	3/8	61.12±0.03	38.20±0.03	22.93±0.03
	1/2	60.75±0.02	37.71±0.02	23.03±0.02
High B2	0	63.94±0.02	38.13±0.02	25.81±0.02
	3/8	61.85±0.02	37.26±0.02	24.60±0.02

Table 9.2: The final acceptances for the different conditions.

Bibliography

[1] D. Britton et al., Phys. Rev. **D49**, 28 (1994).

[2] A. Sher, Tn 6: Possible test of the in/out scattering during the august 2006 beam test: G4 mc simulations of different geometries., Technote, TRIUMF - PiENu, 2007.

[3] K. Yamada, Current analysis summary of dec06 beamtest, Technote, TRIUMF - PiENu, 2007.

[4] A. Sher, Pienu: Measurement of the $\pi \to e\nu$ / $\pi \to \mu\nu$ branching ratio - technical report, Technote, TRIUMF - PiENu, 2008.

[5] W. Marciano and A. Sirlin, Phys. Rev. Lett. **71**, 3629 (1993).

[6] D. Bryman et al., Phys. Rev. **D33**, 1211 (1986).

[7] D. Britton et al., Phys. Rev. Lett. **68**, 3000 (1992).

[8] G. Czapek et al., Phys. Rev. Lett. **17**, 70 (1993).

[9] D. Bryman, Comments Nucl. Part. Phys. **21**, 101 (1993).

[10] D. Bryman and T. Numao, Study of the decay $\pi \to e\nu$, TRIUMF - PiENu Experiment Proposal, 2006.

[11] A. Sher, Objectives of the august beamtest., Technote, TRIUMF - PiENu, 2007.

[12] D. Griffiths, *Introduction to Elementary Particles*, Wiley, John and Sons, Inc., New York, first edition, 1987.

[13] S. Berman, Phys. Rev. Lett. **1**, 468 (1958).

[14] T. Kinoshita, Phys. Rev. Lett. **2**, 477 (1959).

[15] T. Goldman and W. Wilson, Phys. Rev. **D15**, 709 (1977).

[16] W. Marciano and A. Sirlin, Phys. Rev. Lett. **36**, 1425 (1976).

[17] W.-M. Y. et al., J. of Phys. **33**, 1 (2006).

Appendix A

Raw Data

Start	Stop	Insert	e^+	μ^+	π^+	Total
1431	1437	3/8	164072	174417	358387	1082692
1472	1483	3/8	49949	145209	322909	727657
1517	1562	0	47333	134180	318514	698340
1563	1586	1/8	49631	139601	322363	718463
1587	1607	1/4	50419	146416	319254	727589
1608	1621	3/8	86832	270459	564080	1184209
1622	1640	0	54843	162064	368485	788820
1641	1659	3/8	74268	227200	485085	1041198
1660	1682	0	58857	171092	395707	847745
1683	1702	3/8	48531	143022	305918	705563
1703	1712	0	47513	134886	306141	681485
1713	1781	1/2	51641	153335	316006	742808
1796	1859	3/8	144057	224833	378956	988647
1860	1931	0	165161	236613	402003	1040873

Table A.1: The raw data used to compute the beam properties. Note that the total number of events exceeds the sum of the other three columns - the composition percentages were normalized.

Start	Stop	Insert	B2 Magnet	Current	T2	T2&T4	T2&!T4	Total
1431	1437	3/8	High	High	99101	61521	37580	164939
1472	1483	3/8	Normal	Normal	560587	351224	209363	917154
1517	1562	0	Normal	Normal	2178896	1354807	824089	3442569
1563	1586	1/8	Normal	Normal	1121777	703052	418725	1799127
1587	1607	1/4	Normal	Normal	1001856	628453	373403	1624731
1608	1621	3/8	Normal	High	662457	411145	251312	1065755
1622	1640	0	Normal	Normal	946074	584643	361431	1487335
1641	1659	3/8	Normal	High	1002122	622845	379277	1628296
1660	1682	0	Normal	Normal	1033781	637721	396060	1631086
1683	1702	3/8	Normal	Normal	989946	617771	372175	1619514
1703	1712	0	Normal	Normal	512407	317104	195303	809060
1713	1781	1/2	Normal	Normal	3187786	1979177	1208609	5247788
1796	1859	3/8	High	High	2819985	1698579	1121406	4559084
1860	1931	0	High	High	4047034	2413626	1633408	6329614

Table A.2: The raw data used to compute the acceptances.

Appendix B

Suggested Improvements

The TDC thresholds are set very low to minimize the timing-slew due to the pulse shape; however, this makes them very susceptible to noise. As a result, the TDC's tend to record an extremely large number of events, making them hard to interpret and basically useless. I would suggest using a discriminator in addition to the low threshold trigger, to reduce slew while also discarding unwanted noise.

Second, the total energy deposited in the target is an extremely valuable quantity; however, it is very difficult, if not impossible, to achieve. The trigger gate for most of the runs was 450ns whereas the wide gate ADC was only 350ns. Thus, for late decays, the positron exit is not seen and the total energy in the target is unknown. I would suggest lengthening the ADCw gate to the length of the trigger gate to circumvent this problem.